Title

Effect of carbon nanotube alignment on nanocomposite sensing performance

Journal

Materials Research Express, 7(4)

ISSN

2053-1591

Authors

Lee, BM

Huang, Z

Loh, KJ

Publication Date

2020-04-01

DOI

10.1088/2053-1591/ab8842

Peer reviewed

Effect of carbon nanotube alignment on nanocomposite sensing performance

Bo Mi Lee[1,2], Zachary Huang[2], and Kenneth J. Loh[2,*]
[1] Department of Computer Science, University of California Davis, Davis, CA 95616, USA
[2] Department of Structural Engineering, University of California San Diego, La Jolla, CA 92093-0085, USA

[*]E-mail: kenloh@ucsd.edu

Abstract. The objective of this study is to derive a numerical model of carbon nanotube (CNT)-based thin films that accurately reflect their electrical and electromechanical performance as observed through experimental tests. Although nanocomposites based on CNTs dispersed in polymer matrices have been studied extensively, their nanocomposite properties vary depending on CNT orientations. This study aimed to explain how differences in nanocomposite behavior could be explained by numerical models considering different CNT alignment conditions. First, a percolation-based thin film model was generated by randomly dispersing CNT elements in a predefined two-dimensional domain. The degree of CNT alignment in the film was controlled by limiting the CNT elements' maximum angle they make with respect to the film's longitudinal axis. Then, numerical simulations on CNT-based film models were conducted. Second, multi-walled carbon nanotube (MWCNT)-epoxy films were prepared via drop casting. Alternating current was applied to the MWCNT-epoxy mixture before curing to prepare films with different degrees of CNT alignment. The electrical and electromechanical properties of these specimens were characterized, and the results were compared with simulations. Good agreement between experiments and simulations was observed.

Keywords: alignment, carbon nanotube, electromechanical, nanocomposite, orientation, percolation, simulation, strain sensing

1. Introduction

One-dimensional (1D) nanostructured materials, such as nanotubes [1], nanowires [2], and nanorods [3], are characterized by high length-to-diameter aspect ratios. As a result of their 1D structure, they have chemical, electrical, mechanical, and optical properties that differ from other materials. For example, gold (Au) nanorods show two surface plasmon resonance bands due to the oscillation of electrons in longitudinal and transverse axes, while Au nanospheres have just one absorption band. The longitudinal plasmon resonance can be tuned from the visible to the near infrared (NIR) region by adjusting the aspect ratio of the Au nanorods. The plasmon resonance in the NIR region makes them ideal optical probes for *in vivo* imaging, because NIR radiation can penetrate up to 10 cm in tissue with minimal attenuation by water [4-6]. Wang *et al.* [4] demonstrated *in vivo* imaging of single Au nanorods flowing through the blood vessels of a mouse's ear. Nanowires can be segmented into multiple parts consisting of different materials, which allow the wires to perform several tasks [7]. Salem *et al.* [8] assembled bi-segmented Au-nickel nanowires for non-viral gene delivery by attaching the DNA-cell-targeting protein to different segments. Other 1D nanomaterials, including carbon nanotubes (CNT) [9] and silicon nanowires [10], transport electrons almost without scattering, showing near-ballistic electron transport due to their size quantization effects. This results in their high electrical conductivities.

To take advantage of the unique material properties of 1D conductive nanostructured materials in tangible length scales, they have been dispersed in polymer matrices to form nanocomposites. In fact, the electrical properties of polymer matrices can be improved significantly with the inclusion of minute amounts of 1D conductive nanomaterials such as metal nanofibers, carbon nanofibers, and CNTs. Ramasubramaniam *et al.* [11] achieved a low percolation threshold (0.05 wt%) of single-walled carbon nanotubes (SWCNT)-poly(phenyleneethynylene) composites. Sandler *et al.* [12] assembled well-dispersed multi-walled carbon nanotubes (MWCNT) in an epoxy and achieved an extremely low percolation threshold of 0.0025 wt%.

The electrical properties of CNT-based nanocomposites can also be employed to achieve strain sensors where their electrical properties change when subjected to applied strains. Vemuru *et al.* [13] assembled a freestanding MWCNT-based buckypaper film and attached the film onto a brass substrate. The brass specimen was subjected to uniaxial tensile strains to 1,200 με, while the voltage of MWCNT films were simultaneously measured using a four-point probe method. A linear electromechanical or strain sensing response was observed. Christ *et al.* [14] assembled MWCNT-polyurethane (PU) nanocomposites using fused deposition modeling and investigated their strain sensing response while varying MWCNT concentrations from 2 to 5 wt%. The results showed that the 2 wt% MWCNT-PU nanocomposite had the highest strain sensitivity, S (of ~176), while S of the 5 wt% MWCNT-PU nanocomposite was ~8.6. Park *et al.* [15] fabricated 0.56 vol% MWCNT-polyethylene oxide films, where the MWCNT concentration was near the percolation threshold. Uniaxial tensile strains to 1% was applied, and its electrical resistance increased linearly until 0.8% before transitioning to a nonlinear resistance response.

In addition, experimental studies conducted on CNT-based nanocomposites have showed that their electrical and electromechanical performance could be affected by CNT alignment. Khan *et al.* [16] assembled aligned MWCNT-epoxy nanocomposites by applying direct current (DC) of 200–1,200 V. The applied DC voltage allowed CNT bundles to align in the direction of the electric field, and the results showed that aligning MWCNTs resulted in a lower percolation threshold and higher conductivity than composites with randomly distributed MWCNTs. Parmar *et al.* [17] fabricated 5 wt% MWCNT-polycarbonate (PC) composites using injection and compression molding techniques. The electrical resistance of the randomly dispersed MWCNT-PC specimen was lower (740 Ω) than that of the aligned MWCNT-PC specimen (13.9 kΩ). However, strain sensing tests revealed that the aligned specimen was more sensitive to strains with a higher strain sensitivity of 3.65, than the randomly dispersed specimen (S = 2.62). Oliva-Aviles *et al.* [18] applied an alternating current (AC) electric field to align MWCNTs in a polysulfone (PSF) matrix. Optical microscope images showed aligned MWCNTs within the PSF matrix

when the AC electric field (E_{AC} = 7.3 kV/m and f = 60 Hz) was applied to 0.5 wt% MWCNT-PSF nanocomposites. The specimen with aligned MWCNTs was more sensitive to mechanical strains (S = 2.78) as compared to the control specimen where S = 1.57.

To advance the understanding of the relationship between CNT alignment and the bulk film's electrical and electromechanical behavior, numerical simulations on nanocomposite models were explored. Du *et al.* [19] modeled CNT-based nanocomposites by dispersing 1D CNT elements in a 2D space and calculated bulk electrical conductivity as a function of different alignment conditions. The highest conductivity was observed for a slightly aligned CNT nanocomposite model rather than a randomly dispersed CNT network. For example, a 1 wt% CNT-based nanocomposite model produced the highest electrical conductivity when the angles between the CNT element and the y-axis were limited to 60°. This critical angle was varied depending on the CNT concentration. Bao *et al.* [20] computed the electrical conductivity of a 3D percolation-based CNT network model by considering the intrinsic CNT resistance and the contact resistance caused by electron ballistic tunneling at the contact junction. Similar to Du *et al.* [19], the maximum conductivity was observed with partially aligned CNTs. Gong *et al.* [21] found anisotropic electrical properties in aligned CNT-polymer nanocomposites by calculating the conductivities parallel and perpendicular to the CNT alignment direction. Despite the extensive electrical behavior simulations, numerical studies on electromechanical behavior remains rather limited. For example, Hu *et al.* [22] simulated the electromechanical behavior of a CNT network considering different alignment conditions. It was demonstrated that the resistance change ratio increased as CNTs were more aligned to the loading direction.

Therefore, the main objective of this work was to leverage numerical simulations to investigate how CNT alignment affects their bulk electrical and electromechanical performance. This study starts with the implementation of two-dimensional (2D) percolation-based CNT nanocomposite models. CNTs were modeled as straight elements to consider their orientation effects exclusively. Upon model generation by randomly depositing CNTs within a predefined 2D domain space, the electrical resistance of the model was calculated. Then, the model's strain sensitivity was determined using electrical resistance data corresponding to when the film was subjected to different strain states. To experimentally validate the numerical model, MWCNT-epoxy nanocomposites were fabricated by mold casting. The specimens were subjected to uniaxial tensile cyclic strains to evaluate their strain sensing properties. The study concludes by discussing the comparison between the experimental and numerical results.

2. Numerical methods

2.1. Model generation

A 2D percolation-based CNT nanocomposite model was implemented to simulate how CNT orientations influenced bulk film electrical and strain sensing properties. This study builds on the foundation demonstrated in previous studies in which percolation-based models were derived by randomly dispersing CNT elements within a predefined 2D space [23, 24]. Unique in this study was consideration of alignment, and CNTs were assumed to be straight linear segments to better consider how orientation affects the bulk film electrical and electromechanical properties. The degree of CNT-network alignment was described by limiting the maximum angle (θ_{max}) between the longitudinal axis (y) and the CNT axis as shown in figure 1. Here, CNTs were modeled as 1D elements, and the diameter of CNTs was not specified [25, 26]. The orientation of each CNT was then defined by the angle θ between the CNT axis and the x axis (equation 1). In doing so, each CNT can be randomly located within the maximum angle of θ_{max}.

$$\theta = 90 + 2\theta_{max}(rand - 0.5) \quad (1)$$

For example, θ_{max} = 90° described the completely random dispersion of CNTs in the film. As θ_{max} decreased, CNTs were more aligned with the y-axis or the direction of electrical measurements.

Upon defining CNT orientations, the position of each CNT was defined by its two end-points (x_1, y_1) and (x_2, y_2) in a Cartesian coordinate system. One end of the CNT was randomly located within the model space (10×24 μm^2), while the other end was calculated using its length (L_{CNT}) and orientation angle (θ):

$$x_2 = x_1 + L_{CNT}\cos\theta \quad (2)$$

$$y_2 = y_1 + L_{CNT}\sin\theta \quad (3)$$

The procedure was iterated until the predefined number of CNTs (N) was generated. A Gaussian distribution of CNT lengths (*i.e.*, with a mean: 1.904 μm and standard deviation: 0.506 μm) was applied to the model. The length and standard deviation used here were determined based on statistical image analysis of films fabricated [23]. A representative model with $\theta_{max} = 20°$ and $N = 900$ is shown in figure 1.

2.2. Electrical and electromechanical simulations

With the nanocomposite model generated, its electrical resistance was then calculated. First, the algorithms searched for locations of CNT-to-CNT junctions and stored the junction coordinates in a matrix. Then, each CNT element's resistance (R) was calculated by:

$$R = R_{int} + R_{Ohmic} + R_{jct} \quad (4)$$

where R_{int} is the theoretical intrinsic resistance of a CNT in a perfect contact condition (6.5 kΩ), R_{Ohmic} is the Ohmic resistance that depends on the junction-to-junction length, and R_{jct} is the junction resistance. Junction resistance is the contact resistance caused by a tunneling effect between a pair of CNTs at the point of the junction, and it can vary depending on the electrical properties of CNTs (*i.e.*, metallic or semiconducting [27]) and the distance between a pair of CNTs [28]. In this study, an effective contact resistance of 240 kΩ [29] was assumed to be the junction resistance, where metallic-metallic CNTs are separated with a van der Waals distance [30] to be consistent with the use of MWCNTs in the experiments (where only metallic-metallic junctions exist).

Upon calculating the element resistance, its reciprocal was used to build a conductance matrix of the entire CNT network. It was assumed that the electrodes were located at the top and bottom of the CNT nanocomposite model with an applied potential difference of 10 V. Kirchhoff's current law was then employed using the applied voltage and the conductance matrix to determine nodal voltages. The nodal voltages and element resistance were used to compute the total current propagating through the entire CNT-network. The electrical resistance of the CNT network was determined using the total current and the voltage applied to the model [23, 24].

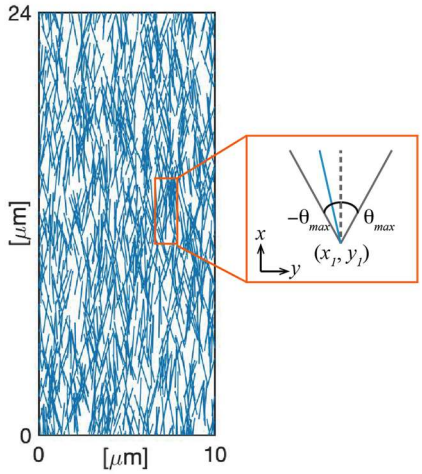

Figure 1. A representative CNT-based nanocomposite model shows straight CNTs were generated within the predefined maximum angle of θ_{max} ($N = 900$ and $\theta_{max} = 20°$).

In addition, the strain sensing behavior of the CNT nanocomposite models was simulated by subjecting the model to uniaxial tensile-compressive strains. The intrinsic strain sensitivity of CNTs was also integrated in the model (where $S_{CNT} = 150$) [31]. At each strain state, the coordinates of each CNT in the network were updated assuming that mechanical strain was applied uniformly throughout the entire nanocomposite while taking into consideration of Poisson's effect:

$$x' = x - \nu\varepsilon\left(x - \frac{W}{2}\right) \tag{5}$$

$$y' = y(1+\varepsilon) \tag{6}$$

where x' and y' are the updated coordinates of the CNT, x and y are the initial unstrained coordinates of the CNT, W is film width, ε is applied strain, and ν is Poisson's ratio of the polymer matrix.

3. Numerical simulation results

In this study, four different CNT orientation conditions of θ_{max} = 20°, 35°, 60°, and 90° were simulated following the procedures discussed in section 2. First, the percolation threshold of each model, defined as the number of CNTs needed to reach the percolation probability of ~ 50% [32], was simulated. The percolation thresholds for models with θ_{max} = 20°, 35°, 60°, and 90° were N = 830, 820, 800, and 780, respectively, indicating that, as CNTs were more aligned to the longitudinal direction, more CNTs were required to construct electrically conductive pathways. Here, 50 models were simulated for each CNT density case for calculating percolation threshold to consider model to model variations.

Based on the percolation threshold results, the unstrained electrical resistance of the model was simulated with the minimum CNT density of N = 850 so that the model's electrical properties could be evaluated. In figure 2, the model's electrical resistance normalized by the maximum model resistance (*i.e.*, corresponding to the average model resistance where N = 900 and θ_{max} = 20°) was plotted as a function of N, where the error bars correspond to the standard deviation of each dataset. During numerical simulations, seven CNT densities (N = 900, 1,100, 1,200, 1,350, 1,550, 1,800, and 2,000) were considered. The results showed that the models became more conductive and decreased in resistance as more CNTs were included, which is consistent with previous studies [23, 33]. This result is expected, because more CNTs distributed in the domain can create denser electrical conducting pathways, thereby increasing bulk electrical conductance and decreasing electrical resistance. In addition, their electrical properties were sensitive to the degree of CNT alignment. For example, at the lowest CNT density considered (N = 900), the model with θ_{max} = 20°

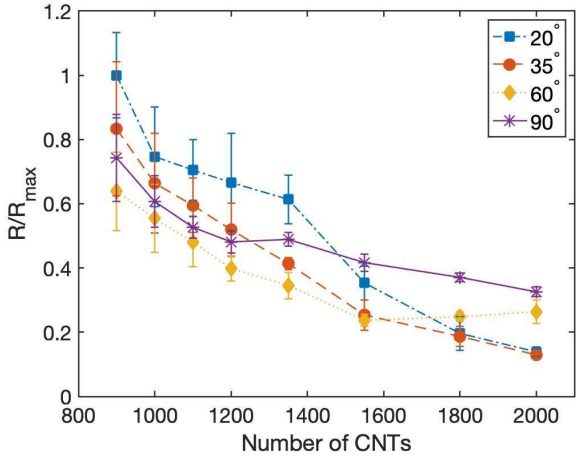

Figure 2. The normalized resistances of CNT-based nanocomposite models with different CNT orientation conditions (θ_{max} = 20°, 35°, 60°, and 90°) were simulated.

showed the highest electrical resistance among models with four different alignment conditions. Models with $\theta_{max} = 60°$ were always more conductive than the model with randomly dispersed CNTs ($\theta_{max} = 90°$) regardless of CNT density.

To better investigate how the electrical property of the CNT nanocomposite models changed with respect to alignment, their normalized resistance was plotted as a function of θ_{max} (figure 3). When $N = 900–1,550$, normalized resistance decreased as θ_{max} increased but then increased for $\theta_{max} = 90°$. This transition occurred at lower θ_{max} for higher CNT densities (*i.e.*, $N = 1,800$ and 2,000), and these results were consistent with other numerical studies [19, 25]. A possible explanation of this transition is that, as the degree of CNT alignment increases, there is a fundamental competition between a decrease in the number of junctions indicating the loss of conducting pathways and a decrease in the length of conducting paths favorable for current flow.

The strain sensing properties of CNT nanocomposite models were also evaluated. Each model was subjected to uniaxial tensile-compressive strains to $\pm 1\%$ at 0.25% increments. Figure 4 plots the

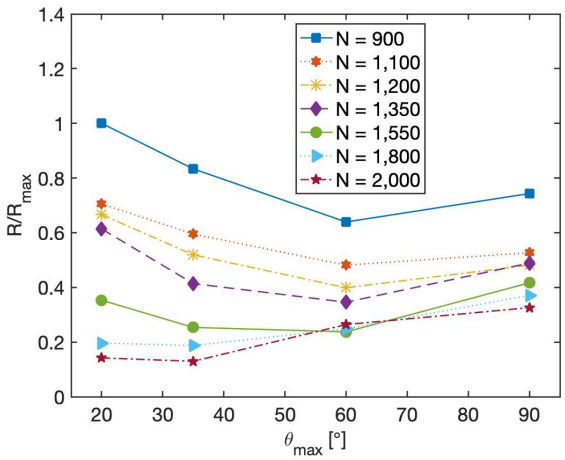

Figure 3. The normalized resistances of CNT-based nanocomposite models were plotted as a function of θ_{max}.

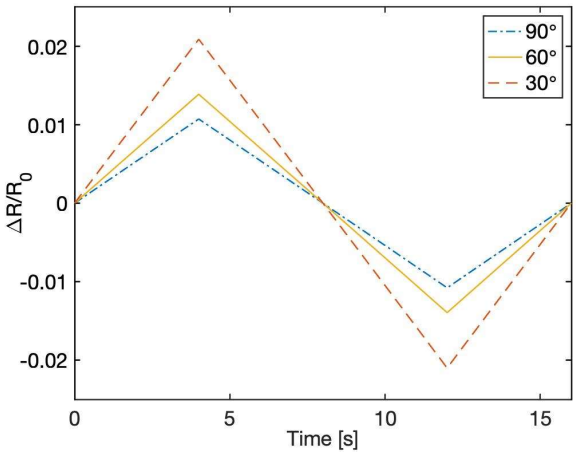

Figure 4. Strain sensing responses of CNT-based nanocomposite models ($N = 1,100$) with different CNT alignment conditions ($\theta_{max} = 90$, 60, and 30) were simulated.

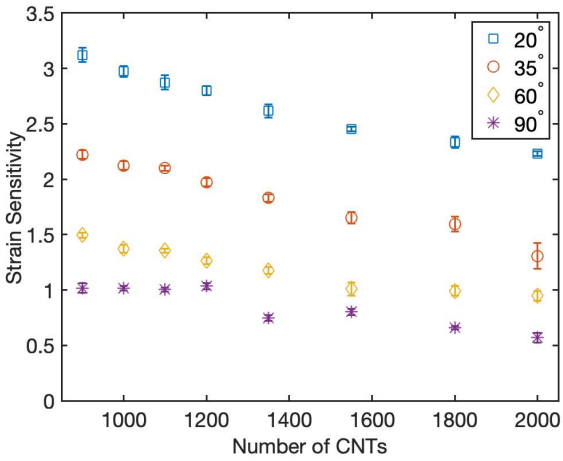

Figure 5. Strain sensitivities of CNT-based nanocomposite models were simulated as a function of CNT density and different CNT alignment conditions.

normalized change in resistance (R_{norm}) of three representative thin film models (θ_{max} = 20°, 60°, and 90°) of the same CNT density (N = 1,100):

$$R_{norm} = \frac{\Delta R}{R_0} \tag{7}$$

where R_0 is the initial unstrained resistance, and ΔR is the change in resistance of the CNT model at each applied strain state with respect to its unstrained baseline resistance. It can be seen that R_{norm} changed linearly with respect to applied strains. To quantitatively compare the strain sensing performance of models with different θ_{max} conditions, strain sensitivity of the bulk film model was defined as follows:

$$S = \frac{R_{norm}}{\Delta\varepsilon} \tag{8}$$

where $\Delta\varepsilon$ is the change in applied strains. Strain sensitivity is equal to and determined from the slope of the linear least-squares best-fit line to each dataset, and the results are summarized in figure 5. Similar to the simulation results for the unstrained cases, CNT density was varied (N = 900, 1,100, 1,200, 1,350, 1,550, 1,800, and 2,000). It can be seen that S decreased as CNT density increased, which is consistent with previous results [23, 24] and other experimental and numerical findings [34, 35]. In particular, strain sensitivity results were affected by the degree of CNT alignment. As CNTs became more aligned to the direction of loading (as θ_{max} decreased), the CNT nanocomposite model was more sensitive to applied strains. According to the numerical simulation results, one can expect that CNT-based nanocomposites with aligned CNTs would be more sensitive to strains. These numerical simulation results will be compared with experimental thin film characterization tests, which will be explained in the next sections.

4. Experimental methods

4.1. Materials

MWCNTs were purchased from NanoIntegris Technologies Inc. UV-curable epoxy (OG198-54) was acquired from EPO-TEK®. Dragon Skin® FX-Pro (Dragon Skin) was acquired from Smooth-On.

4.2. Nanocomposite fabrication

MWCNT-epoxy specimens were fabricated using a drop casting fabrication method. First, epoxy resin was added to MWCNTs to obtain four different MWCNT concentrations (*i.e.*, 0.15, 0.2, 0.3, and 0.4 wt%). The mixture was then subjected to high-speed shear mixing for 5 min at 3,500 rpm. To enhance their dispersion, the MWCNT-epoxy mixture was also subjected to high-energy tip sonication (3 mm tip, 50 W, 22 kHz).

(a) (b)

Figure 6. (a) An MWCNT-epoxy film was fabricated; and (b) it was mounted in the load frame for characterizing its strain sensing behavior.

The procedure of shear mixing and tip sonication was repeated four times to uniformly disperse MWCNTs without agglomerations.

The MWCNT-epoxy mixture was casted in a 60 × 10 × 1 mm^3 Dragon Skin rectangular mold. AC voltage was applied to the mixture to create aligned MWCNTs using a dielectrophoresis effect [36]. The AC electric field induces the translational force and torque on suspended polarizable particles (*i.e.*, MWCNTs) surrounded by a dielectric medium (*i.e.*, epoxy matrix) resulting in aligned MWCNTs [18, 37, 38]. Two electrodes were prepared by attaching aluminum tape on polyethylene terephthalate films; then, they were fixed to opposite ends of the mold while keeping their separation distance fixed. AC voltages of 0.5 and 1.5 kV at f = 30 kHz was applied to the electrodes for 10 min, yielding electric fields of E_{AC} = 8.3 and 25 kV/m^{-1}, respectively. After AC voltage was applied for 9 min, the mixture was cured using an ultraviolet (UV) light source (Uvitron Porta-ray 400W) applied for 1 min (while still applying the AC electric field). Additional heat treatment of the specimens was conducted in a Yamato ADP-300C oven for 12 h at 65°C to cure areas that were not adequately exposed to UV light. Once the specimens were fully cured, two electrodes were established at opposite ends of the specimen using copper tape strips for two-point probe electrical measurements. The length between two electrodes was 24 mm. Silver paste was applied over the copper tape electrodes and the specimens to minimize contact impedance (figure 6(a)).

4.3. Strain sensing characterization

The MWCNT-epoxy films were mounted in a Test Resources 150R load frame for strain sensing characterization (figure 6(b)). The load frame applied 1 N of preload to keep the specimen taut. Prior to strain sensing tests, the unstrained (baseline) resistance of each film was measured using a Keysight 34401A digital multimeter. The gage length between the two grips of the load frame was 40 mm. Then, the load frame executed a three-cycle uniaxial tensile load pattern to a maximum strain of 1% (strain rate: 1%/min) while simultaneously measuring its electrical resistance response. Electrical resistant measurements and the load frame's crosshead displacement were recorded using the Keysight BenchVue data logging software.

5. Experimental results

The unstrained or nominal electrical resistance measurements of MWCNT-epoxy films are plotted in figure 7. Each data point corresponds to the average unstrained electrical resistance calculated from five independent measurement sets. As the MWCNT concentration increased from 0.15 to 0.5 wt%, their unstrained resistance decreased (*i.e.*, MWCNT-epoxy films became more conductive). In addition, AC

voltage conditions affected the bulk-film electrical properties. When MWCNT concentration was 0.15 wt%, the specimen with 1.5 kV_{p-p} showed higher electrical resistance than the other AC voltage conditions (3.36 MΩ and 7.52 MΩ for 0 and 0.5 kV_{p-p}, respectively). On the other hand, for 0.2 wt%, the electrical resistance was higher (3.57 MΩ) at 0.5 kV_{p-p} as compared to the 0 and 1.5 kV_{p-p} cases (1.72 MΩ and 2.47 MΩ, respectively). This trend was consistent with findings described by the numerical models in section 3.

In this study, electrical properties in both the alignment and nonalignment directions were investigated to evaluate the degree of CNT network alignment. Anisotropic electrical conductivity, in which the resistance parallel to the alignment direction is different than its orthogonal direction, were used to evaluate CNT alignment. For instance, Wang *et al.* [37] assembled highly aligned SWCNT-epoxy nanocomposites by means of unidirectional mechanical stretching, which resulted in highly aligned SWCNTs in the direction of stretching. The results showed that the conductivity in the alignment direction was higher than that of the orthogonal direction. Gong *et al.* [21] simulated CNT-based nanocomposites and presented that the model had higher conductivity along the CNT alignment direction than perpendicular to it. In addition, Ramillard *et al.* [39] investigated electrical anisotropy of aligned MWCNT buckypaper by evaluating the log-ratio of electrical resistance and revealed that the log-ratio increased as MWCNTs were more aligned. Similarly, an electrical resistance ratio (r) was defined and calculated to evaluate the degree of CNT network alignment for the MWCNT-epoxy films tested in this work (equation 9):

$$r = \frac{R_{\perp}}{R_{||}} \tag{9}$$

where $R_{\perp}$ is the resistance perpendicular to the applied AC field, and $R_{||}$ is the resistance parallel to the alignment direction. To measure $R_{\perp}$ and $R_{||}$, MWCNT-epoxy films were cut into 10 × 10 mm^2 specimens, and the resistance in both directions was measured. The results are summarized in figure 8. For each data point, the resistance ratios of three samples were obtained and then averaged. When AC voltage was not applied to the MWCNT-epoxy specimens (0 kV_{p-p}), the resistance ratio was ~ 1, indicating that MWCNTs were uniformly distributed. When AC voltage was applied to the films, electrical anisotropy was confirmed. As the applied voltage increased from 0.5 kV_{p-p} to 1.5 kV_{p-p}, the resistance ratio increased regardless of MWCNT concentrations, thereby validating increased MWCNT alignment, which was also consistent with other studies [21, 37, 39].

By following the procedures described in section 4.3, the strain sensing performance of MWCNT-epoxy specimens was characterized. Figure 9 plots the normalized change in resistance time histories of 0.2 wt% MWCNT-epoxy films subjected to different electric field conditions (0, 0.5, and 1.5 kV_{p-p}). All three specimens showed linear strain sensing properties in response to applied tensile cyclic loading. In addition,

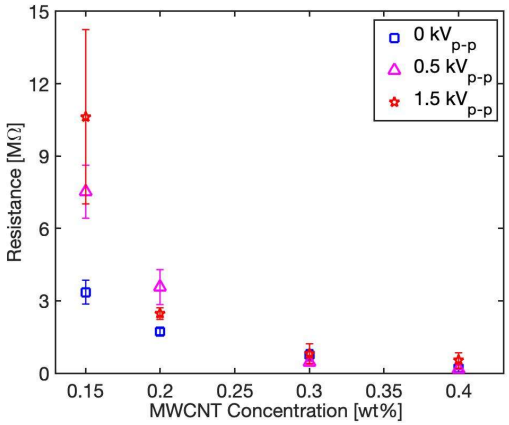

Figure 7. The unstrained electrical resistances (with the standard errors of the mean shown as error bars) of MWCNT-epoxy films are plotted.

the 1.5 kV_{p-p} specimen showed a higher peak normalized change in resistance at the maximum strain (1 %) as compared to the other specimens.

6. Comparison of numerical and experimental results

Sections 3 and 5 showed that both the numerical models and the MWCNT-epoxy films were characterized by linear strain sensing or piezoresistive behavior. For better comparison, the normalized change in resistance of MWCNT-epoxy films and numerical modeling results were plotted together as a function of applied strain in figure 10. Because compressive strains to experimental specimens would buckle the films, only tensile strain sensing results were considered in this study and shown in figure 10. The experimental results were presented as data points, whereas numerical simulation results were plotted as linear lines. It can be clearly seen that the slope of the lines increased as the applied voltage increased (for the experiments) and as θ_{max} decreased (for simulations). Overall, good agreement was observed between the numerical simulation results and experimental test data.

The strain sensitivity results of the models and the MWCNT-epoxy strain sensors were plotted together as a function of CNT density in figure 11. For the experiments, each data point represents the average strain

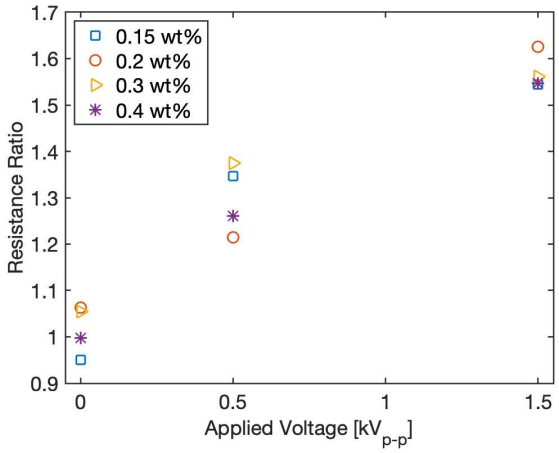

Figure 8. The ratio of electrical resistance of MWCNT-epoxy films was calculated to characterize the effect of the applied electric field.

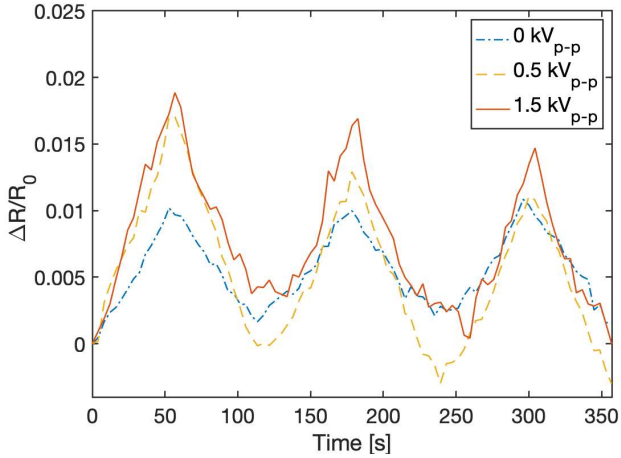

Figure 9. The electrical resistance responses of 0.2 wt% MWCNT-epoxy thin films with different electric field conditions (0 kV_{p-p}, 0.5 kV_{p-p}, and 1.5 kV_{p-p}) are plotted.

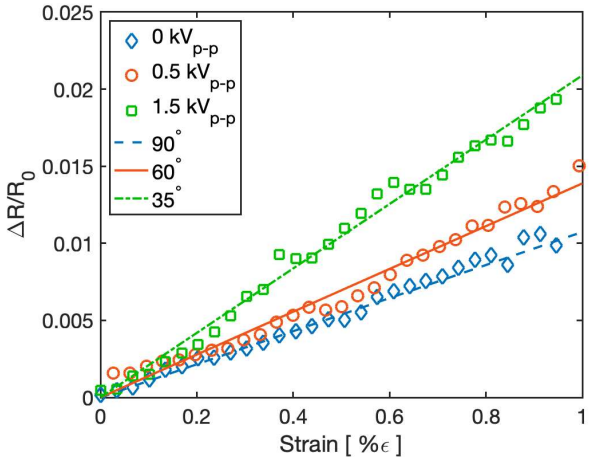

Figure 10. The normalized change in resistance of MWCNT-epoxy films and numerical models is plotted as a function of applied strains.

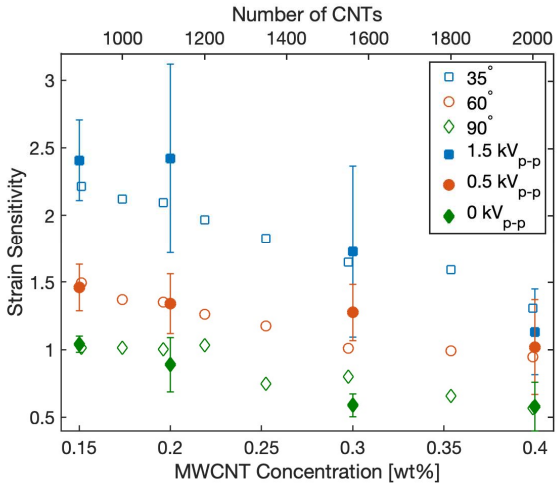

Figure 11. The strain sensitivity results of experimental tests and numerical simulations (with standard errors of the mean shown as error bars) are compared.

sensitivity evaluated obtained from testing five MWCNT-epoxy specimens. From the results, higher MWCNT concentrations had lower sensitivities to applied strains. In addition, specimens subjected to higher AC voltages yielded higher strain sensitivities. One can see that the experimental strain sensitivity results are described by the CNT-based percolation models with different alignment conditions of θ_{max} = 35°, 60°, and 90°. Overall, these results suggest that CNT orientations in nanocomposites significantly affect their strain sensing performance, and there is a clear relationship between the degree of CNT alignment and strain sensitivity. Therefore, CNT nanocomposite models could be potentially used for guiding the design of nanocomposites with specific strain sensing properties through the manipulation of AC alignment field strengths and CNT concentrations.

7. Conclusions

In this study, numerical simulations and experimental investigations of CNT-based nanocomposites were conducted to better understand the relationship between CNT orientations, CNT concentrations, and their bulk electrical and electromechanical performance. First, CNT nanocomposite percolation models that considered different alignment conditions were implemented. Numerical simulations were performed to

evaluate their baseline electrical and strain sensing properties. The modeling results showed that increasing number or density of CNTs improved electrical conductivity. Moreover, CNT alignment affected bulk film electrical resistance. Second, MWCNT-epoxy films were then fabricated by drop casting. To obtain aligned films, high AC electric voltage was applied to the MWCNT-epoxy mixture after pouring them into the mold but just before the curing process. Sample sets with four different MWCNT concentrations and three different magnitudes of applied AC voltages were prepared. The unstrained electrical resistance of each specimen was measured, and their electromechanical property was evaluated by subjecting the specimen to tensile cyclic loading. From the electromechanical tests, the results showed that the electrical resistance ratio increased as applied AC voltage increased, thereby validating different degrees of MWCNT alignment in the film. Finally, the simulation results were then compared with experimental findings. Both the modeling and MWCNT-epoxy film test results confirmed their linear piezoresistivity. The results also showed that nanocomposite strain sensitivity increased as CNTs were more aligned to the direction of loading. Furthermore, good agreement between the models and experiments was found. The models were able to accurately describe the strain sensing response of MWCNT-epoxy films, and comparable strain were observed.

Acknowledgements
This research was supported by the US National Science Foundation (NSF) under grand number CMMI CAREER 1253564. Additional support was also provided by the Jacobs School of Engineering, University of California San Diego.

References

[1] Iijima S 1991 Helical microtubules of graphitic carbon *Nature* **354** 56-8
[2] Wu B, Heidelberg A and Boland J J 2005 Mechanical properties of ultrahigh-strength gold nanowires *Nat. Mater.* **4** 525-9
[3] Yu Y-Y, Chang S-S, Lee C-L and Wang C R C 1997 Gold nanorods: electrochemical synthesis and optical properties *J. Phys. Chem. B* **101** 6661-4
[4] Wang H, Huff T B, Zweifel D A, He W, Low P S, Wei A and Cheng J-X 2005 In vitro and in vivo two-photon luminescence imaging of single gold nanorods *Proceedings of the National Academy of Sciences of the United States of America* **102** 15752-6
[5] Imura K, Nagahara T and Okamoto H 2004 Plasmon mode imaging of single gold nanorods *J. Am. Chem. Soc.* **126** 12730-1
[6] Mackey M A, Ali M R K, Austin L A, Near R D and El-Sayed M A 2014 The most effective gold nanorod size for plasmonic photothermal therapy: theory and in vitro experiments *J. Phys. Chem. B* **118** 1319-26
[7] Wang J 2009 Biomolecule-functionalized nanowires: from nanosensors to nanocarriers *ChemPhysChem* **10** 1748-55
[8] Salem A K, Searson P C and Leong K W 2003 Multifunctional nanorods for gene delivery *Nat. Mater.* **2** 668-71
[9] White C T and Todorov T N 1998 Carbon nanotubes as long ballistic conductors *Nature* **393** 240-2
[10] Nehari K, Cavassilas N, Autran J L, Bescond M, Munteanu D and Lannoo M 2006 Influence of band structure on electron ballistic transport in silicon nanowire MOSFET's: An atomistic study *Solid State Electron.* **50** 716-21
[11] Ramasubramaniam R, Chen J and Liu H 2003 Homogeneous carbon nanotube/polymer composites for electrical applications *Appl. Phys. Lett.* **83** 2928-30
[12] Martin C A, Sandler J K W, Shaffer M S P, Schwarz M K, Bauhofer W, Schulte K and Windle A H 2004 Formation of percolating networks in multi-wall carbon-nanotube–epoxy composites *Compos. Sci. Technol.* **64** 2309-16

[13] Vemuru S M, Wahi R, Nagarajaiah S and Ajayan P M 2009 Strain sensing using a multiwalled carbon nanotube film *J. Strain Anal. Eng.* **44** 555-62
[14] Christ J F, Aliheidari N, Ameli A and Pötschke P 2017 3D printed highly elastic strain sensors of multiwalled carbon nanotube/thermoplastic polyurethane nanocomposites *Materials & Design* **131** 394-401
[15] Park M, Kim H and Youngblood J P 2008 Strain-dependent electrical resistance of multi-walled carbon nanotube/polymer composite films *Nanotechnology* **19** 055705
[16] Khan S U, Pothnis J R and Kim J-K 2013 Effects of carbon nanotube alignment on electrical and mechanical properties of epoxy nanocomposites *Compos. Part A Appl. Sci. Manuf.* **49** 26-34
[17] Parmar K, Mahmoodi M, Park C and Park S S 2013 Effect of CNT alignment on the strain sensing capability of carbon nanotube composites *Smart Mater. Struct.* **22** 075006
[18] Oliva-Avilés A I, Avilés F and Sosa V 2011 Electrical and piezoresistive properties of multi-walled carbon nanotube/polymer composite films aligned by an electric field *Carbon* **49** 2989-97
[19] Du F, Fischer J E and Winey K I 2005 Effect of nanotube alignment on percolation conductivity in carbon nanotube/polymer composites *Phys. Rev. B* **72** 121404
[20] Bao W S, Meguid S A, Zhu Z H and Meguid M J 2011 Modeling electrical conductivities of nanocomposites with aligned carbon nanotubes *Nanotechnology* **22** 1-8
[21] Gong S, Zhu Z H and Meguid S A 2015 Anisotropic electrical conductivity of polymer composites with aligned carbon nanotubes *Polymer* **56** 498-506
[22] Hu N, Karube Y, Arai M, Watanabe T, Yan C, Li Y, Liu Y and Fukunaga H 2010 Investigation on sensitivity of a polymer/carbon nanotube composite strain sensor *Carbon* **48** 680-7
[23] Lee B M, Loh K J and Yang Y-S 2017 Carbon nanotube thin film strain sensor models assembled using nano- and micro-scale imaging *Comput. Mech.* **60** 39-49
[24] Lee B M and Loh K J 2017 Carbon nanotube thin film strain sensors: comparison between experimental tests and numerical simulations *Nanotechnology* **28** 1-14
[25] Behnam A and Ural A 2007 Computational study of geometry-dependent resistivity scaling in single-walled carbon nanotube films *Phys. Rev. B* **75** 125432
[26] Rahman R and Servati P 2012 Effects of inter-tube distance and alignment on tunnelling resistance and strain sensitivity of nanotube/polymer composite films *Nanotechnology* **23** 1-9
[27] Baughman R H, Zakhidov A A and de Heer W A 2002 Carbon nanotubes-the route toward applications *Science* **297** 787-92
[28] Buldum A and Lu J P 2001 Contact resistance between carbon nanotubes *Phys. Rev. B* **63** 161403-1-4
[29] Fuhrer M S, Lim A K L, Shih L, Varadarajan U, Zettl A and McEuen P L 2000 Transport through crossed nanotubes *Physica E* **6** 868-71
[30] Fuhrer M S, et al. 2000 Crossed nanotube junctions *Science* **288** 494-7
[31] Cao J, Wang Q and Dai H 2003 Electromechanical properties of metallic, quasimetallic, and semiconducting carbon nanotubes under stretching *Phys. Rev. Lett.* **90** 157601
[32] Zeng X, Xu X, Shenai P M, Kovalev E, Baudot C, Mathews N and Zhao Y 2011 Characteristics of the electrical percolation in carbon nanotubes/polymer nanocomposites *J. Phys. Chem. C* **115** 21685-90
[33] Lee B M and Loh K J 2015 A 2D percolation-based model for characterizing the piezoresistivity of carbon nanotube-based films *J. Mater. Sci.* **50** 2973-83
[34] Amini A and Bahreyni B 2012 Behavioral model for electrical response and strain sensitivity of nanotube-based nanocomposite materials *J. Vac. Sci. Technol.* **30** 022001
[35] Pham G T, Park Y-B, Liang Z, Zhang C and Wang B 2008 Processing and modeling of conductive thermoplastic/carbon nanotube films for strain sensing *Compos. B. Eng.* **39** 209-16
[36] Xue W and Li P 2011 Dielectrophoretic deposition and alignment of carbon nanotubes *Carbon nanotubes - synthesis, characterization, applications*, ed S Yellampalli (Rijeka, Croatia InTech) pp 171-90

[37] Wang Q, Dai J, Li W, Wei Z and Jiang J 2008 The effects of CNT alignment on electrical conductivity and mechanical properties of SWNT/epoxy nanocomposites *Compos. Sci. Technol.* **68** 1644-8
[38] Brown D A, Kim J-H, Lee H-B, Fotouhi G, Lee K-H, Liu W K and Chung J-H 2012 Electric field guided assembly of one-dimensional nanostructures for high performance sensors *Sensors* **12** 5725-51
[39] Remillard E M, Zhang Q, Sosina S, Branson Z, Dasgupta T and Vecitis C D 2016 Electric-field alignment of aqueous multi-walled carbon nanotubes on microporous substrates *Carbon* **100** 578-89